Decoupled nuclei and nuclear polar rings in regular spiral galaxies. NGC 2841[*]

O.K. Sil'chenko[1], V.V. Vlasyuk[2], and A.N. Burenkov[2]

[1] Sternberg Astronomical Institute, University av. 13, Moscow 119899, Russia
[2] Special Astrophysical Observatory, Nizhnij Arkhyz, Karachaj-Cherkess Republic, 357147 Russia

Abstract. The Sb galaxy NGC 2841 was observed at the 6 m telescope of SAO RAS with the Multi-Pupil Field Spectrograph and at the 1 m telescope of SAO RAS with the long-slit spectrograph. An unresolved nucleus of NGC 2841 is shown to be chemically decoupled both in magnesium and in iron with abundance break estimates of 0.36 dex for Mg and 0.6 dex for Fe; an abundance gradient in the bulge is seen only in the magnesium index and is typical for early-type disk galaxies. The rotation axis of the nuclear ionized gas in NGC 2841 is perpendicular to that of the central stellar population; an existence of a bulge stellar component with decoupled rotation momentum in the radius range $5''$-$12''$ is suspected. A possible scenario for the origin of the unusual central structure in NGC 2841 is proposed.

Key words: galaxies: NGC 2841; nuclei; stellar content; structure; kinematics and dynamics; abundances

1. Introduction

Chemically and kinematically decoupled galactic nuclei have been known for some years, but mostly in elliptical galaxies (Jedrzejewski & Schechter 1988; Bender 1988; Bender & Surma 1992; Davies et al. 1993; Carollo & Danziger 1994). Early hypothesis related this phenomenon to a merger of a smaller stellar system. Later when it became clear that decoupled nuclei in elliptical galaxies may be nuclear disks (Surma & Bender 1995), a variant of dissipative merging was proved to be better.

Several years ago we claimed the existence of chemically decoupled nuclei in spiral galaxies for the first time (Sil'chenko et al. 1992). We had obtained equivalent width radial profiles up to several arcseconds from the center by measuring the MgIλ5175 absorption line in three early-type spiral galaxies, NGC 615,

7013, and 7331, where earlier we had detected dynamically decoupled nuclei, namely, strong central mass concentrations (Afanasiev et al. 1989). It seemed that in the central parts of their bulges any magnesium-strength gradients were absent inside the error limits; but the nuclei were decoupled, showing a higher magnesium-line strength at the level of 2σ and more. The values of metallicity differences between the decoupled nuclei and the surrounding bulges ranged from a factor of two to almost an order of magnitude. Obviously a dissipationless merging was to be excluded in the case of decoupled nuclei in spiral galaxies.

We have begun a systematic search for chemically distinct nuclei in galaxies by composing a list of galaxies with photometrically distinct nuclei. Among 234 early-type galaxies with detailed multi-aperture photoelectric data which were found in the catalogues of Longo and de Vaucouleurs (1983, 1985) about 25% of ellipticals and lenticulars and about 50% of early-type spirals show nuclei which are prominently redder that the neighbouring bulges (Sil'chenko 1994). So it may be possible that chemically distinct nuclei are a rather common phenomenon. We have selected 34 objects of the northern sky for a detailed investigation. As dust concentration may also provide the red colour of the nuclei, bidimensional spectroscopy was necessary to prove the dynamical and chemical distinctness of nuclei in these galaxies. So we started an observational program with the Multi-Pupil Field Spectrograph (MPFS) of the 6 m telescope (Special Astrophysical Observatory, Nizhnij Arkhyz, Russia). Now we have completed and published results on two galaxies from this list. The elliptical galaxy NGC 1052 appears to possess a resolved chemically decoupled core with a radius of $3''$ (300 pc); the ionized gas inside this radius co-rotates with the stars whereas the gas further outward rotates (and is distributed) orthogonally to the stars (Sil'chenko 1995). The small spiral galaxy NGC 4826 has become famous during last three years by its counterrotating outer gaseous disk: the sense of gas rotation suddenly changes at the radius of 1 kpc (Braun et al. 1994; Rubin 1994; Rix et al. 1995). We have found an unresolved chemically distinct nucleus in this galaxy; the central gas rotates circularly and together with the stars (Sil'chenko 1996). Though only two arbitrary examples may not be representative,

---

some suspicions have arisen that the phenomenon of chemically decoupled nuclei can be related to external gas capture.

NGC 2841 was chosen as having a photometrically distinct red nucleus (Sil'chenko 1994). But it has one more property which is interesting for us. When we found the first three chemically decoupled nuclei in spiral galaxies (Sil'chenko et al. 1992), in all three early-type spiral galaxies possessing such nuclei the orientation of the innermost isophotes was shown to be the same as that of the outermost isophotes; in other words, their bulges look axisymmetrical (Sil'chenko & Vlasyuk 1992). And in NGC 2841 any turn of the isophote major axis was thought to be absent too (Mizuno & Hamajima 1987) so this galaxy was one of the best our candidates for possessing a chemically distinct nucleus. Besides, it was known to have a compact photometric nucleus whose brightness exceeded an extrapolation of the de Vaucouleurs' bulge (Kormendy 1985).

2. Observations and data reduction

Spectral observations of the center of NGC 2841 were carried out in the Special Astrophysical Observatory of RAS (Nizhnij Arkhyz, Russia) with the Multi-Pupil Field Spectrograph (MPFS), installed in the prime focus of the 6-meter telescope (Afanasiev et al. 1990), and also by using a long-slit spectrograph, attached to the Cassegrain focus of the 1-meter reflector of the Special Astrophysical Observatory. The log of observations is presented in Table 1.

MPFS, which is a second (after CFHT TIGER system, see Bacon et al. 1995) realisation of G. Courtes' (1982) concept of spatial sampling of extended sources by means of a microlens array, has been in active operation at the 6-meter telescope since 1989. Instruments of this type are providing sufficient gain in investigations of nebulae and galaxies with respect to a classical slit spectroscopy due to complete coverage of studied sky area, independence of spectral resolution on spatial resolution, absence of slit losses and of the overall problem of object matching.

A set of enlargers, which project the object onto the lens array, provide spatial sampling according to seeing value — from $\approx 0.3''$ to $\approx 1.7''$ per lens. Sizes of the used array varied between 9×11 and 8×16 elements. We have chosen for our observations the $10x$ enlarger, providing a scale of 1.3–$1.4''$ per lense and a field of view of $\approx10\times16''$ for different instrument setups. The accurate scale values and sizes of field of view are given in Table 1.

We have exposed two sets of spectra in the green spectral range ($\lambda\lambda$ 4700–5500 Å) with a spectral resolution near 6 Å and one set of spectra in the red wavelength range ($\lambda\lambda$ 6450–6700 Å) with a resolution about 2 Å.

To account accurately for the night sky background in the green spectral range we have separately exposed the blank sky region at $1.5'$-$2'$ from the galaxy with an exposure time of one half of that for the galaxy; the sky was then (after spectrum extraction and linearization) smoothed and subtracted.

The hollow-cathode lamps filled by He-Ne-Ar or Ne-Xe-Ar gas mixtures were exposed before and after each exposure in order to provide wavelength calibration of spectral data. Integrations of the twilight sky were carried out for correcting system vignetting and variations of the transmission by the individual lenses.

The long-slit spectrograph was installed at the Cassegrain focus of the 1 meter Zeiss reflector and equipped by a fast (f/1.5) Schmidt-Cassegrain camera and large-format CCD (1040×1160 elements). The four cross-sections at different position angles were accumulated with spatial sampling $1.54''$ per pixel at a spectral resolution of 4Å and over the spectral range of 4100-6000 Å. In order to clean spectral accumulations from cosmic ray hits all exposures were divided in two. For wavelength calibration we have used Ne-Xe-Ar lamps exposed before and after each object exposure.

The basic data reduction steps – bias subtraction, flatfielding, cosmic ray hits removing, extraction of one-dimensional spectra, transformation into wavelength scale, construction of surface brightness maps and velocity fields – were performed using the software developed in the Special Astrophysical Observatory (Vlasyuk 1993).

The green spectra obtained with MPFS were used to construct maps of surface brightness in the continuum at $\lambda5100$ and two-dimensional velocity fields for the stellar component (only the spectra obtained with CCD in 1996 are suitable for cross-correlation; as a template, we have taken the spectrum of the nucleus). Then the spectra of individual elements were added in the rings centered on the nucleus; the width of the rings was equal to the lens size and the step between neighbouring rings was also equal to the lens size. These summarized spectra were used to derive radial dependencies of absorption line strengths – main attention was paid to Hβ, MgIb, and Fe lines $\lambda5270$ and $\lambda5335$.

The red spectra were only used to derive a velocity field and a spatial distribution of the ionized gas: the long exposure has allowed us to measure weak emission lines Hα and [NII]$\lambda6583$ in the center of NGC 2841 for the first time.

Long-slit spectra obtained at the 1 m telescope were tentatively destined to confirm the properties of the velocity fields obtained with MPFS: as the slit was very broad, $s = 4''$, the measured picture appears to be slightly smoothed, and there are problems with exact localization of measured features.

From these data we estimate an accuracy of stellar and gas velocities as 20 km s^{-1} and an accuracy of absorption-line equivalent widths as 0.3 Å for the spectra registered with IPCS and as 0.1 Å for the spectra registered with CCD.

The benefit of the Multi-Pupil Field Spectrograph over the long-slit spectrographs in the study of absorption line radial dependencies is that after summing spectra in the rings, we deal with a radially constant level of accumulated counts and do not need to apply logarithmic binning to obtain the constant equivalent-width accuracy over all the radii under consideration.

3. Chemically decoupled nucleus in NGC 2841

Fig. 1 presents radial profiles of the well-known absorption-line index Mgb (for the absorption-line index definitions – see

Table 1. Spectral observations of NGC 2841

Date	Telescope	Configuration	Exposure	Field	Scale	PA of long side	Seeing
20/21.10.93	6m	MPFS+IPCS 512 × 512	21 min	$12'' \times 14''$	1.27''/lens	152°	1.5''
25/26.10.94	6m	MPFS+CCD 520 × 580	90 min	$14'' \times 22''$	1.35''/lens	−12°	2''
12/13.01.96	1m	LS+CCD 1040 × 1160	60 min	$4'' \times 3'$	1.54''/pixel	152°	3.7''
13/14.01.96	1m	LS+CCD 1040 × 1160	60 min	$4'' \times 3'$	1.54''/pixel	242°	3''
14/15.01.96	1m	LS+CCD 1040 × 1160	60 min	$4'' \times 3'$	1.54''/pixel	92°	2''
14/15.01.96	1m	LS+CCD 1040 × 1160	60 min	$4'' \times 3'$	1.54''/pixel	122°	2''
27/28.02.96	6m	MPFS+CCD 1040 × 1160	60 min	$17'' \times 22''$	1.43''/lens	166°	3.5''
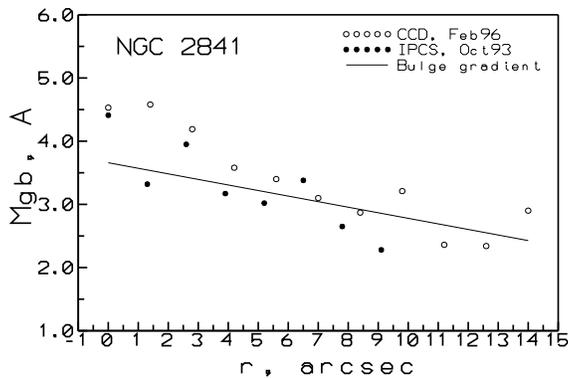
Fig. 1. The magnesium-line radial dependence in the center of NGC 2841.

Worthey et al. 1994), measured in the center of NGC 2841 twice: in 1993 and in 1996. As was mentioned above, the indices measured with IPCS are far less accurate than those measured with CCD, but in this case the two independent data sets agree perfectly. The only discrepancy at $r = 1.3''$ can be explained by the seeing difference (see Table 1). Two conclusions can be derived by examining Fig. 1: firstly, it is the first case during our search for chemically decoupled nuclei where a rather strong magnesium-strength gradient in the bulge is present, and secondly, the unresolved nucleus is decoupled by its increased Mg-line strength even if we extrapolate the metallicity trend in the bulge towards $r = 0$. The straight line in Fig. 1 shows the least-square fit to the bulge magnesium-line trend in the radius range $4''–14''$. It is just the bulge, because according to recent photometric data of Varela et al. (1996) the bulge dominates in NGC 2841 up to $r \approx 50''$ (its $r_e = 25''$). The formula of the straight line in Fig. 1 is

$$Mgb = (3.66 \pm 0.25) - (0.088 \pm 0.031)r'',$$

so the nucleus which has $Mgb = 4.47 \pm 0.06$ is distinguished from the underlying bulge at a confidence level of more than 3σ, and the metallicity break calibrated by using the models of old stellar populations from Worthey (1994) is equal to 0.36 dex. By applying the same metallicity-Mgb relation to the Mgb gradient in the bulge, we obtain $d[\text{m/H}]/d\log r = -0.9 \pm 0.3$. Balcells & Peletier (1994) investigated metallicity gradients in
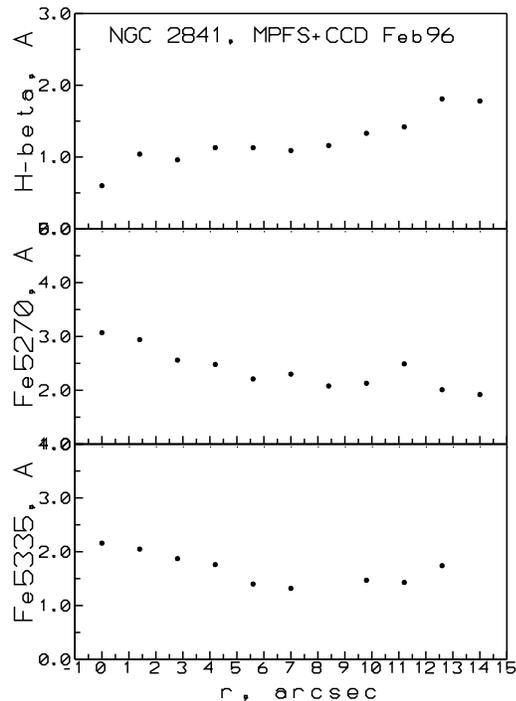
Fig. 2. The Balmer absorption and iron-line radial dependencies in the center of NGC 2841.

bulges of early-type disk galaxies by considering profiles of the broad-band color $B - R$, and they have reported a range of metallicity gradients from 0 to –1. So our result for NGC 2841 is consistent with the mean characteristics of early-type disk galaxies.

Here we must note that a linear Mgb dependence on r in the central bulge is not physically conditioned – it is only the most exact and convenient presentation in this range of radius. For example, if we apply a logarithmic relation, the fit would be less accurate by a factor of two. As the structure of the bulge of NGC 2841 may be very complex and inhomogeneous (see the next Section), we prefer not to restrict ourselves by any physical model but rather to use a good empirical relation.

Fig. 2 presents radial dependences of other three absorption-line indices resulting from our CCD observations with MPFS. We see that the nucleus of NGC 2841 is also decoupled from the bulge by increased strength of the Fe lines; but the gradient of
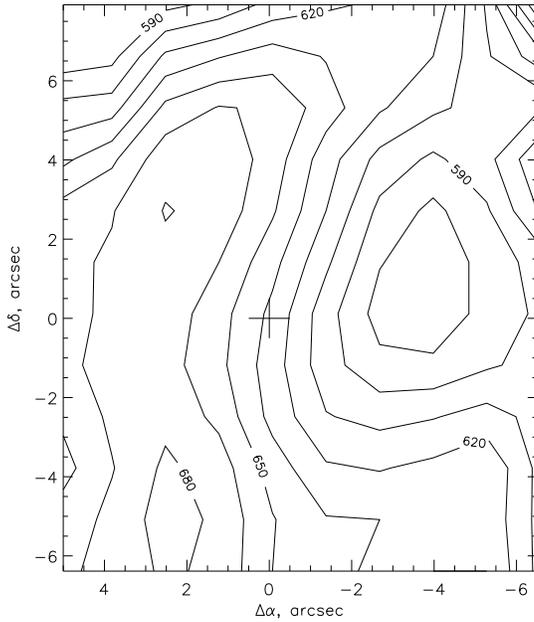
Fig. 3. The isovelocities of ionized gas in the center of NGC 2841. The cross marks the photometric center of the galaxy. North is up, east is to the left.

Fig. 4. The isovelocities of stars in the center of NGC 2841 with respect to the systemic velocity of the galaxy. The cross marks the photometric center of the galaxy. North is up, east is to the left.

the Fe line strengths in the bulge is quite negligible. The *Fe5270* difference between the nucleus and the bulge (0.9 ± 0.3Å) corresponds to the metallicity difference $\Delta[Fe/H] = 0.6 \pm 0.2$ dex (by using the calibration of Worthey 1994). The slight depression of the $H\beta$ absorption line in the central region of NGC 2841 results from its contamination by emission. Overall, the small point-to-point scatter in Fig. 2 confirms the high accuracy of the present index determinations (r. m. s. is 0.1 Å, as mentioned above).

4. Stellar and gaseous kinematics in the center of NGC 2841

Figs. 3 and 4 presents isovelocities for the gaseous (October 1994) and stellar (February 1996) velocity fields in the center of NGC 2841 (the stellar velocities are given with respect to the systemic velocity, because the cross-correlation is made with the nuclear spectrum as a template). For isovelocity continuity, the derived velocity fields were smoothed by a gaussian with $FWHM \approx 3''$; as for the stellar velocity field, the smoothing has not affect the spatial resolution because of rather poor seeing during the observations of February 1996, but the maximum gas rotation velocity is in reality slightly higher than is seen in Fig. 3.

From the MPFS spectra, obtained in October 1994 at a rather good spectral resolution (2 Å) in the $H\alpha$ spectral region, we have estimated a nuclear gas velocity dispersion as 170 km s^{-1}. The nuclear stellar velocity dispersion is known to be of the same order: 220 km s^{-1} (Delisle & Hardy 1992). So we expected to find stellar and gaseous rotation with comparable velocity amplitudes. The rotations of both components are clearly seen in Figs. 3 and 4, but their characters are quite different: the ionized gas rotates perpendicular to the stellar component. Another dif-
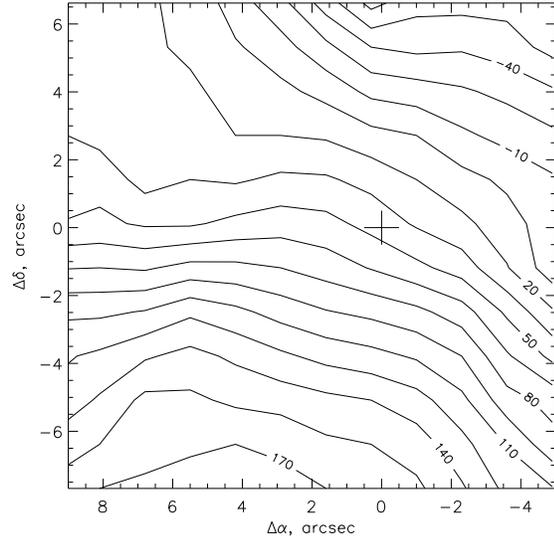
ference concerns the location of the rotation velocity maxima: the gaseous component demonstrates two prominent velocity extremes – one negative and one positive with respect to the systemic velocity – 3.8$''$ from the center, and the stellar component rotates like a solid body inside the radius of 6$''$. If the dynamical center of the gaseous component lies between the rotation-velocity extremes, it is shifted from the photometric center by about 2$''$. It is difficult to judge if the difference between the dynamical and photometric center positions is real: the extremes of the gas velocity field are probably related to the edge of the nuclear gaseous polar disk, because at 4.5$''$ from the (dynamical) center the zero-velocity line suddenly turns by 90$°$, and the gas further outward obviously rotates together with the stars.

Let us try to determine the orientations of the rotation axes more exactly. Under the assumption of circular rotation, an azimuthal dependence of central line-of-sight velocity gradients must be a pure cosine curve with a maximum at the orientation of the line of nodes PA_0:

$$dv_r/dr = \omega \sin i \cos (PA - PA_0),$$

where ω is a deprojected angular rotation velocity and i is an inclination of the rotation plane. Two-dimensional velocity fields give an unique opportunity to study such dependencies in detail. Fig. 5 presents azimuthal dependencies of central line-of-sight velocity gradients for the gaseous (unsmoothed) and stellar (smoothed) velocity fields. The center is defined as photometric center, the range in radius defined by two conditions – to be inside the solid-body area and to provide the maximum of measured directions – is 2.8$''$–4$''$.

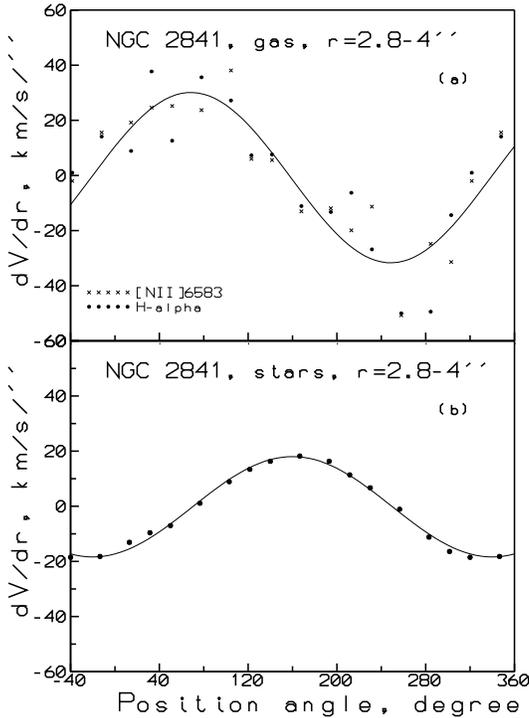The cosine laws calculated by the least-square method are

Fig. 5. Azimuthal dependencies of the central line-of-sight velocity gradients for NGC 2841 obtained with MPFS. The solid lines show cosine curves fitted by the least-square method.

Fig. 6a and b. Azimuthal dependencies of the central line-of-sight velocity gradients for NGC 2841 obtained with the long-slit spectrograph. The solid lines show cosine curves fitted by the least-square method.

$$dv_r/dr = [30.9 \cos(PA - 68°) - 0.8] \text{ km s}^{-1} \text{ arcsec}^{-1},$$

for the gaseous component and

$$dv_r/dr = [18.2 \cos(PA - 160°) - 0.2] \text{ km s}^{-1} \text{ arcsec}^{-1},$$

for the stellar component. We see that the rotation axes of both components are indeed orthogonal. The difference of cosine curve amplitudes may be related to different inclinations of rotation planes, but more likely it results from the smoothing of the stellar velocity field. The overall shapes of the azimuthal dependencies in Fig. 5 resemble cosine laws very closely, so we conclude that a circular rotation may be the dominant component for both velocity fields, stellar and gaseous. The low-amplitude wave oscillations of points around the cosine curve in the PA range $120° - 280°$ in Fig. 5a may be real because they are seen in both Hα and [NII]λ6583; if this is the case, a small bar may be present in the center of NGC 2841. This possibility will be discussed in the next section.

As we have mentioned above, four long-slit cross-sections were obtained for NGC 2841 at the 1 m telescope in the position angles 152° (major axis), 242° (minor axis), 92°, and 122° to verify the properties of the stellar velocity field. A weak emission line [OIII]λ5007 has appeared to be quite measurable inside $r \approx 5''$ in these spectra. Fig. 6 presents an analog of Fig. 5, but obtained with the long-slit spectrograph of the 1 m telescope. To compensate for a low count level, we have measured the spec-
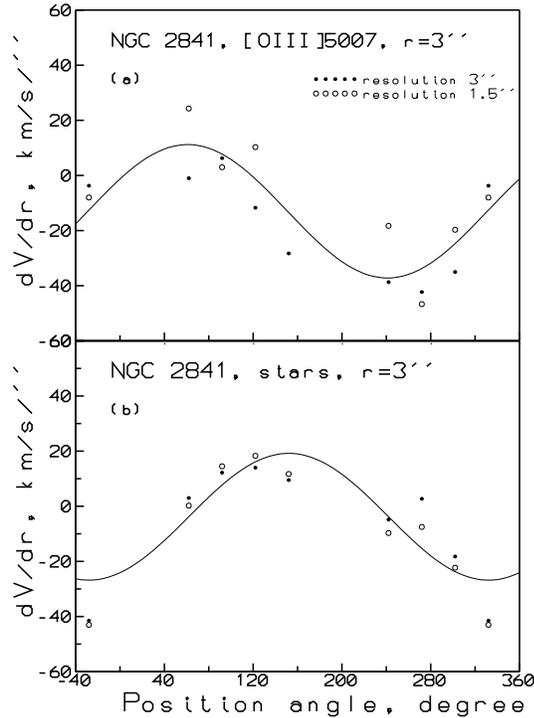
tra twice: each individual row (a spatial element of 1.54″) and binning by 2 rows (a spatial element of 3.1″). The agreement of the two measurements is satisfactory. The fitted cosine laws in Fig. 6 are

$$dv_r/dr = [24.2 \cos(PA - 61°) - 13] \text{ km s}^{-1} \text{ arcsec}^{-1},$$

for the gaseous component and

$$dv_r/dr = [23 \cos(PA - 152°) - 3.8] \text{ km s}^{-1} \text{ arcsec}^{-1},$$

for the stellar component. Though the number of directions involved in Fig. 6 is much less than in Fig. 5, the orthogonality of the rotation planes of the gaseous and stellar components is fully confirmed. The angular rotation velocities for gas and stars are almost equal here, the spatial resolutions being equal, so our initial expectation of the comparable rotation velocity amplitudes for the gas and stars due to their comparable velocity dispersions is justified.

Fig. 7 presents a comparison of the major-axis and minor-axis stellar velocity cross-sections with the earlier measurements of Whitmore et al. (1984) and Fillmore et al. (1986). To obtain a higher accuracy of velocity measurements, we have cross-correlated separately two fragments of spectra – in the wavelength ranges 4800–5320 ÅÅ and 5320–5840 ÅÅ, – and each with two spatial binnings, of 1.54″ and of 3.1″, so we had four measurements at each radius which being averaged have
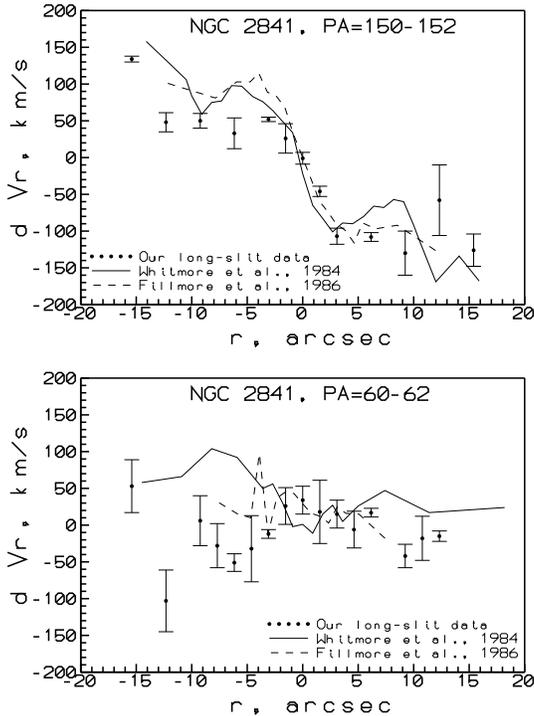
Fig. 7. Comparison of our long-slit cross-sections along the major ($PA = 150° − 152°$) and the minor ($PA = 60° − 62°$) axes with earlier measurements of Whitmore et al. (1984) and of Fillmore et al. (1986).

Fig. 8. Long-slit line-of-sight stellar velocity profiles obtained at the 1 m telescope. Fat straight lines indicate fits to the observational data in the radius ranges of $0''$–$3.5''$ and (only for PA 92° and 242°) of $4.5''$–$10''$.

allowed us to estimate intrinsic errors in the means shown in Fig. 7. An independent check of the wavelength scale accuracy was made by measuring the night-sky emission line [OI]λ5577. After leaving aside systematic velocity differences of 20 km s^{-1} (major axis) and 10 km s^{-1} (minor axis), the agreement of our measurements with previous ones may be accepted as satisfactory, though one must keep in mind that their slits were much narrower than ours.

The results for the all four position angles are presented in Fig. 8. The curves have been shifted in velocity to reach a maximum symmetry for the distributions to the left and to the right from the nucleus. To show how successful this procedure is, in Fig. 8 we present, in addition to the real profiles (dark symbols), the curves mirrored about $r = 0$ (light symbols). In three cross-sections out of four, the nucleus has a line-of-sight velocity systematically higher than the calculated systemic velocity (the excess is from 20 to 40 km s^{-1}). It may be explained by an uncertainty of slit positioning with respect to the kinematical center of the galaxy due to a finite (large enough) slit width or by the disagreement between the kinematical and photometic centers mentioned above. But another effect seems to be more interesting: in two cross-sections, $PA = 92°$ and $PA = 242°$, there are indications of a counterrotating component in the radius range of $5''$–$12''$. Some low-amplitude motions were earlier measured along the minor axis without any comments (Whitmore et al. 1984; Fillmore et al. 1986), but after symmetrization it appears that we deal with systematic solid-body rotation (projected ro-
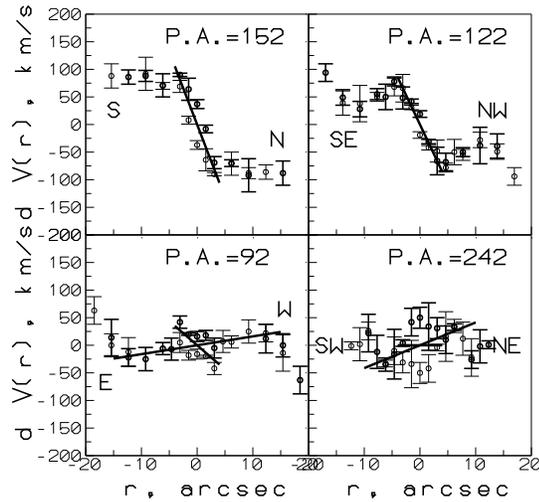
tation velocity at $r_{pr} = 6''$ along the minor axis of the galaxy is 40 km s^{-1}) of which the rotation axis does not coincide with that of more inner and more outer parts of the galaxy. In Fig. 8, $P.A. = 92°$, this counterrotating (conditionally counterrotating because the projected velocity along the minor axis is not zero) component is seen even better. It lies between $r = 4.5''$ and $r = 10''$ and demonstrates a slow solid-body rotation – slower than that of the kinematically decoupled core inside $r \approx 3''$. It could be a projection effect; alternatively, the component could really be dynamically hotter than the nucleus.

Finally, Fig. 9 presents a rotation curve of the stellar component of NGC 2841 which is calculated over the MPFS and the long-slit data. The two-dimensional field shown in Fig. 4 was fitted by a circular rotation model; the best parameters defining the orientation of the plane of rotation – $PA_0 = 155°$ and $i = 60°$ – were used to calculate the rotation curve shown in Fig. 9. Besides this curve, two long-slit cross-sections closest to the major axis were reduced to the plane of the galaxy with the same orientation parameters. All three curves show rather good agreement. The local rotation-velocity maximum at $r = 4.5''$ reported earlier by Whitmore et al. (1984) and Fillmore et al. (1986) is seen but looks far less prominent than in the data of our precursors. Instead, a higher velocity maximum has appeared at $r = 6'' − 10''$. We will not to stress the problem of the exact location of the local maximum of the rotation velocity. It is more important that the analysis of the stellar velocity field reveals that the central region of NGC 2841 is kinematically distinct, and the radius of this kinematically decoupled core – $r = 3'' − 4''$ – is only an upper limit because of poor seeing (of order of $3''$–$4''$ too).
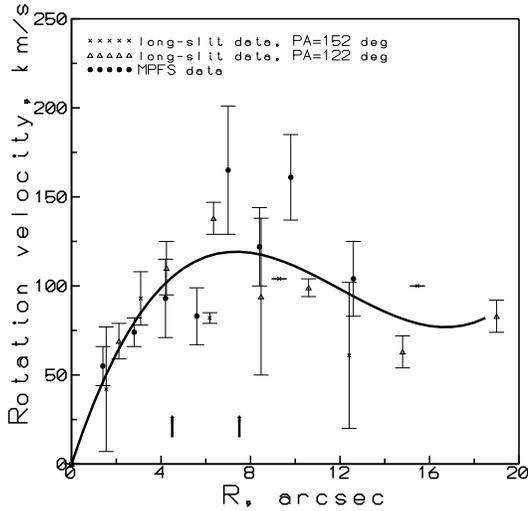
Fig. 9. Composite rotation curve of the center of NGC 2841 calculated by using the data obtained with MPFS and with the long slit. The solid curve show fitting by a third-order polynomial. Arrows mark the locations of "old" (mentioned by Whitmore et al.1984, and by Fillmore et al. 1986) local rotation velocity maximum and of the "new" one found in this paper.

5. May be a nuclear bar?

Both visible effects, the counterrotation and the local velocity maxima, can in reality be artifacts produced by a triaxial compact structure in the center of NGC 2841. The best way to verify if there is a nuclear bar in the galaxy is to trace the orientation of isophotes towards the center. If the structure is axisymmetrical, the position angle of isophote major axis would be constant over all the radii; if there is a bar, the isophote major axis would turn (the only exception – when a bar is aligned with the line of nodes – can be excluded because such a configuration results in a plateau on the line-of-sight velocity profile along the major axis which is not observed in NGC 2841).

Fig. 10 presents results of fitting the isophotes obtained with MPFS by ellipses. Also in the same manner we have fitted isophotes of an NGC 2841 image registered by the (unrepaired) WFPC of the Hubble Space Telescope on September 23/24, 1992 (the exposure time was 260+260 sec, the filter was F555W, the program No. 3912 of S. M. Faber); the image was taken from the HST archive. The characteristics of the outermost isophotes were obtained by using the image of the galaxy from the Digital Sky Survey provided by the SKYVIEW service. All three MPFS exposures have given identical estimates of isophote ellipticities. Though the HST image shows systematically larger ellipticities (by about 0.1) than the MPFS images, the overall trend demonstrated by all the data is monotonous, without any signs of increased ellipticity in the center which must take place in the case of bar presence. The PA dependencies on radius look less definitive. All three data sets obtained with MPFS are quite consistent at $r = 5'' - 6''$: here we have measured $< PA(\text{major axis}) >= 141.5° \pm 1°$. But the orientation of the WFPC isophotes
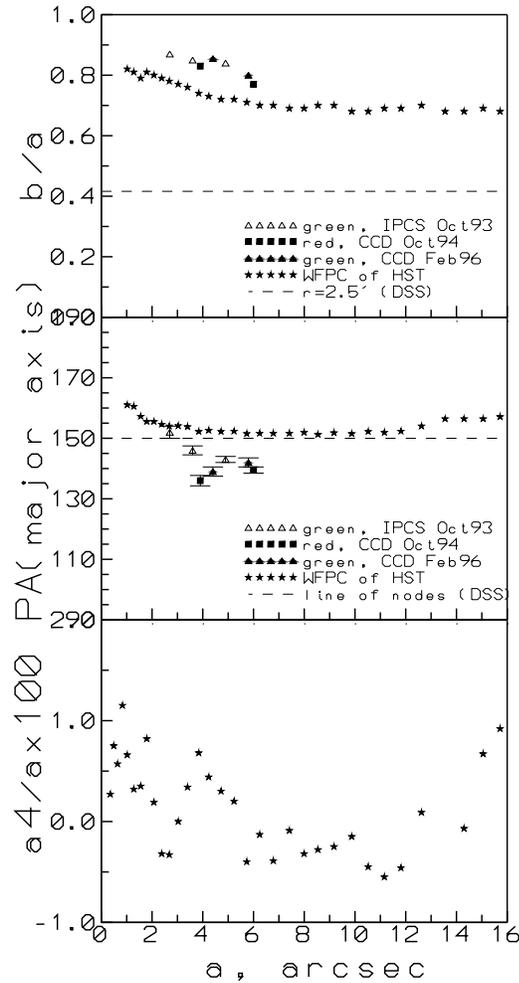

Fig. 10. Radial dependencies of axial ratio, major axis position angle, and boxiness derived from isophotal analysis of the central part of NGC 2841.

in the same radius range is $PA = 152°$, and Varela et al. (1996) give 147°. So we cannot state with certainty that the orientation of the innermost isophotes in NGC 2841 is exactly coincident with the line of nodes; but the turn if it exists is rather small, and in any case there is no nuclear bar perpendicular to the line of nodes (so called "edge-on bar") which alone can mimic circumnuclear rotation velocity maxima and produce a cosine curve dv_r/dr vs. PA with the maximum at the line of nodes (Fig. 5b and 6b). The HST image, $34'' \times 34''$ in the central CCD frame, has also allowed us to estimate the boxiness of the central isophotes up to the radius of about $15''$. In the semi-major axis range of $6''-12''$ the isophotes have a clear boxy shape with the mean $(a_4/a) \times 100 = -0.32 \pm 0.04$. Let us note that this semi-major axis range (taking into account the ellipticity of 0.3) corresponds exactly to the radius range where there is an indication of a kinematically decoupled bulge zone in Fig. 8 ($PA = 92°$ and $242°$).

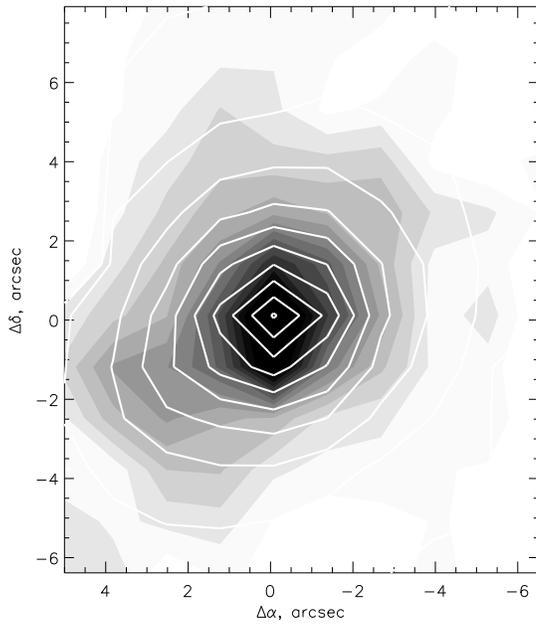Fig. 11 presents a composite image constructed for the central region of NGC 2841 using the MPFS data: the continuum

Fig. 11. The image of the central part of NGC 2841 in the continuum $\lambda 6500$ (white isophotes) and in the emission line [NII]$\lambda 6583$ (grey-scaled contours) obtained with MPFS.

at $\lambda 6500$ and the emission-line intensity for [NII]$\lambda 6583$. While the continuum isophotes look like almost perfect ellipses, without asymmetries or center shift and therefore without any signs of dust presence, the nitrogen emission-line distribution has a rather complex character. Keel (1983) reported that emission in the center of NGC 2841 demonstrated a one-sided bar-like distribution with a PA of $105°$. At a fainter level we have obtained a distribution resembling a two-sided bar, aligned with the line of nodes and quite symmetrical with respect to the nucleus, but with some kind of wings, or lobes, at a $PA \approx 30°$. Interestingly, quite similar lobes with a similar orientation (PA of about $50°$) are seen on the outermost radio-continuum isophotes ($r \approx 3'$) presented by Condon (1987). As the lobes in Fig. 11 do not perfectly coincide with the velocity extremes of the ionized gas (Fig. 3), we are not sure that we see a polar gaseous disk overlapping the main gaseous disk of the galaxy. But some structure perpendicular to the plane of the galactic disk and seen in both ionized gas and radio continuum emission, on scales from the circumnuclear area to the outermost parts of NGC 2841, is obviously present.

6. Discussion and conclusions

In Sect. 3 we have seen that NGC 2841 has a chemically decoupled nucleus. Its presence can be seen from the increased magnesium-line and iron-line strengths. Besides our observations, there are two more facts published earlier but without special comments. Terndrup et al. (1994) present a $J - K$ color profile for NGC 2841 which demonstrates a break of 0.4 mag between the nucleus and the bulge at $r = 3''$ and an absence of

$J - K$ gradient in the radius range $3''$-$100''$. As the broad-band color $J - K$ is related mainly to the iron abundance, the similar behaviour of the *Fe5270* and *Fe5335* profiles in our measurements is in agreement with the results of Terndrup et al. (1994). Also, Delisle & Hardy (1992) have measured radial profiles of absorption lines in the near-infrared spectral range; the CaII IR triplet profile presented for NGC 2841 reveals a break of this absorption line index by more than 1Å between the nucleus and nearby bulge ($r < 8''$). So we consider a chemical distinctness of the nucleus in NGC 2841 as fully confirmed. Here we must only note that the estimates of abundance breaks mentioned in the Sect. 3 – 0.36 dex for the magnesium and 0.6 dex for the iron – are lower limits because of uncertain age of the nuclear stellar population. If the nuclear stellar population is noticeably younger than the bulk of stars in the surrounding bulge, the abundance difference estimates should be increased.

In Sect. 4 we have seen that NGC 2841 has a dynamically decoupled nucleus and an unusual rotation of gas and stars in the outskirts of the nucleus. The gas rotation is strictly perpendicular to that of the nuclear stellar population, and also to the rotation of the global neutral-hydrogen disk of the galaxy – Rots (1980) gives an estimate of the dynamical major axis of the large-scale HI distribution $PA_0 = 155°$. There is an indication of a stellar "counterrotating" component on the long-slit cross-sections in directions far from the major axis, in the radius range $5''$-$12''$. More probably, the mass distribution in the center of NGC 2841 is near-axisymmetrical because of the almost constant orientation of the continuum isophotes. In this case the angular momentum of circumnuclear gas and that of part of the stellar bulge are really decoupled, and these components must have an external origin. We know one more Sb galaxy with a similar set of properties – NGC 7331. It has a chemically decoupled stellar nucleus (Sil'chenko et al. 1992), an axisymmetric nuclear mass concentration traced by a decoupled fast solid-body rotation of the ionized gas (Afanasiev et al. 1989; Sil'chenko & Vlasyuk 1992), and recently a counterrotating stellar component was found in the bulge of NGC 7331 in the radius range $4''$-$15''$ (Prada et al. 1996). The similarity is strong, and as NGC 7331 and 2841 are very nearby galaxies, perhaps, a development of observational tools will lead to a discovery of a whole class of such objects. What can be the cause of such a set of properties?

As we have mentioned in the Introduction, a detection of chemically decoupled nuclei in some galaxies with outer gas of obviously external origin has given rise to an idea over the connection between galaxy interaction and a phenomenon of decoupled nuclei. In the case of NGC 2841 and 7331 the mechanism of galaxy interaction works quite well too. There were numerous hints in the literature that interaction perturbs large-scale gaseous disks of galaxies and provokes intense gas inflows towards nuclei (see, for example, Tutukov & Krugel 1995). A history of NGC 2841 may be the following. Some billions years ago NGC 2841 had experienced an encounter with a smaller gas-rich galaxy and had accreted some amount of its gas with decoupled momentum. The gas of NGC 2841 itself was perturbed and in part settled into the nucleus more quickly than the

accreted external gas (due to more effective dynamical friction in the large-scale disk of NGC 2841). A star formation burst occured in the nucleus, and a secondary chemically decoupled stellar population was produced. The accreted external gas continued to settle towards the center through the bulge, and in some vicinity of the nucleus its density became high enough to begin another star formation burst; the counterrotating part of the bulge had formed. Part of the accreted gas has remained unlocked after this star formation burst and has conserved its "strange" rotation up to date. Such a scenario may be quite universal. In particular, in the frame of this hypothesis NGC 4826 where counterrotating gas lives only at $r > 1.5$ kpc and there is no counterrotating stellar component yet, can be an early stage of NGC 2841 and NGC 7331.

References

Afanasiev V.L., Sil'chenko O.K., Zasov A.V., 1989, A&A 213, L9

Afanasiev V.L., Dodonov S.N.,, Sil'chenko O.K., Vlasyuk V.V., 1990, preprint SAO, N54.

Bacon R., Adam G., Baranne A., et al., 1995, A&AS 113, 347

Balcells M., Peletier R.F., 1994, AJ 107, 135

Bender R., 1988, A&A 202, L5

Bender R., Surma P., 1992, A&A 258, 250

Braun R., Walterbos R., Kennicutt R.C., Jr., Tacconi L.J., 1994, ApJ 420, 558

Carollo C.M., Danziger I.J., 1994, MNRAS 270, 523

Condon J.J., 1987, ApJS 65, 485

Courtes G., 1982, in : Instrumentation for Astronomy with Large Optical Telescopes, ed. by C.M.Humphries, Dordrecht: D.Reidel Publ. Co., p. 123.

Davies R.L., Sadler E.M., Peletier R.F., 1993, MNRAS 262, 650

Delisle S., Hardy E., 1992, AJ 103, 711

Fillmore J.A., Boroson T.A., Dressler A., 1986, ApJ 302, 208

Jedrzejewski R., Schechter P.L., 1988, ApJ 330, L87

Keel W.C., 1983, ApJ 268, 632

Kormendy J., 1985, ApJ 292, L9

Longo G., de Vaucouleurs A., 1983, A General Catalogue of Photoelectric Magnitudes and Colors in the U, B, V System. Austin: Univ. Texas Press

Longo G., de Vaucouleurs A., 1985, Supplement to the General Catalogue of Photoelectric Magnitudes and Colors of Galaxies in the U, B, V System. Austin: Univ. Texas Press

Mizuno T., Hamajima K., 1987, PASJ 39, 221

Prada F., Gutierrez C.M., Peletier R.F., McKeith C.D., 1996, ApJ 463, L9

Rix H.-W. R., Kennicutt R.C., Jr., Braun R., Walterbos R.A M., 1995, ApJ 438, 155

Rots A.H., 1980, A&AS 41, 189

Rubin V.C., 1994, AJ 107, 173

Sil'chenko O.K., 1994, AZh 71, 706

Sil'chenko O.K., 1995, Pis'ma v Astron. Zh. 21, 323

Sil'chenko O.K., 1996, Pis'ma v Astron. Zh. 22, 124

Sil'chenko O.K., Vlasyuk V.V., 1992, Pis'ma v Astron. Zh. 18, 643

Sil'chenko O.K., Afanasiev V.L., Vlasyuk V.V., 1992, AZh 69, 1121

Surma P., Bender R., 1995, A&A 298, 405

Terndrup D.M., Davies R.L., Frogel J.A., De Poy D.L., Wells L.A., 1994, ApJ 432, 518

Tutukov A.V., Krugel E., 1995, A&A 299, 25

Varela A.M., Munoz-Tunon C., Simmoneau E., 1996, A&A 306, 381

Vlasyuk V.V., 1993, Astrofiz. issled. (Izv. SAO RAS) 36, 107

Whitmore B.C., Rubin V.C., Ford W.K., Jr., 1984, ApJ 287, 66

Worthey G., 1994, ApJS 95, 107

Worthey G., Faber S.M., Gonzalez J.J., Burstein D., 1994, ApJS 94, 687